PCCP

Accepted Manuscript

ROYAL SOCIETY OF CHEMISTRY

www.rsc.org/pccp

REACTIVE AND UNREACTIVE PATHWAYS IN A PHOTOCHEMICAL RING OPENING REACTION FROM 2D FEMTOSECOND STIMULATED RAMAN

David T. Valley[1], *David P. Hoffman*[2] *and Richard A. Mathies**

Department of Chemistry, University of California Berkeley, Berkeley, California 94720, United States

*To whom correspondence is addressed
E-mail: ramathies@berkeley.edu
Phone: (510) 642-4192

[1]Current address: Department of Chemical Engineering and Material Science, University of Minnesota – Twin Cities, 421 Washington Ave SE Minneapolis, MN, 55455, United States

[2]Current address: Janelia Research Campus, Howard Hughes Medical Institute, Ashburn, Virginia 20147, United States

Abstract

Two-dimensional femtosecond stimulated Raman spectroscopy (2D-FSRS) is used to probe the structural evolution of a modified cyclohexadiene as it undergoes a photoinduced ring opening reaction. Analysis of the excited state stimulated Raman vibrational data reveals oscillations of the center frequencies and amplitudes of 21 high frequency modes. These oscillations in vibrational properties are due to anharmonic couplings between the high frequency finger print modes and the impulsively driven low frequency molecular distortions in the excited state. The largest anharmonic couplings, with intrinsic oscillation magnitudes of up to 40 cm^{-1}, are observed between the 467 cm^{-1} C-C bend and the 1333 cm^{-1} C-C stretch with the 191 cm^{-1} methyl wag, all of which are centered on the reactive cyclohexadiene moiety. Conversely, motions located on the periphery–the 993 cm^{-1} phenyl bend, the 1389 cm^{-1} methyl bend and 1580 cm^{-1} phenyl C-C stretch–are coupled with the 104 cm^{-1} asymmetric bend. These couplings reveal two key energetic pathways: one leading to formation of the ring-opened product and the other reversion back to the ground state. This work is also important because it presents a new powerful method for measuring anharmonicities of potential energy surfaces and determining their role in chemical reactivity.

Introduction

To understand chemical reactivity it is essential to probe key molecular properties such as the shape of the potential energy surfaces (PES) involved in the reaction, their surface crossings[1] and dynamic energy flow between internal degrees of freedom.[2,3] All of these properties are intimately intertwined as a result of the anharmonic coupling between the molecular normal motions. However, quantitative measurement of the excited state PES shape, in general, and anharmonic couplings, in particular, has proven to be a difficult task. This challenge is addressed here by using two-dimensional femtosecond stimulated Raman (2D-FSRS) to study the

photochemical ring opening of a cyclohexadiene derivative.

One-three cyclohexadiene (CHD) is a classic example of a photochemical ring opening reaction that likely involves large excited state anharmonic coupings.[4] After photoexcitation, CHD exits the Franck-Condon (FC) region along the Raman active and nominally harmonic degrees of freedom before passing through a reactive conical intersection in approximately 80 fs, undergoing a conrotatory mechanism consistent with the orbital symmetry rules developed by Woodward and Hoffman.[5] When the wave packet is in the vicinity of the conical intersection, the potential energy surfaces cannot remain harmonic and the previously independent normal modes strongly couple to one another. Resonance Raman studies of unmodified CHD have highlighted the roles of the olefinic torsion, as well as stretching of the aliphatic C-C bond and the CH_2 twist, in the initial distortions on the reactive excited state surface.[6]

To make this reaction more practically useful and experimentally accessible extensive synthetic work has developed a family of photochromic molecules in which the wavelength of the ring opening is tuned into the visible.[7] These analogues have proven valuable for visible-light actuated molecular switches.[8] Here we focus on 1,2-bis(2,4-dimethyl-5-phenyl-3-thienyl) perfluoro-cyclopentene (ModCHD) the spectral and structural properties of which are summarized in Figure 1. In cyclohexane, ModCHD's absorption spectrum peaks at 560 nm, which is assigned to a $\pi \rightarrow \pi^*$ transition. The cycloreversion quantum yield is reduced from around 50% for CHD to below 5% for the more π-conjugated diarylethenes derivatives. Studies of these derivatives have revealed a transition state (TS) on the excited state before the reactive product determining conical intersection.[9–11] Femtosecond transient absorption studies have assigned a 3 ps time constant to the transit of the excited state wave packet over the TS and a 9 ps constant for the conical intersection that determines photoswitching.[10] The ring closing

reaction of ModCHD, where there are both reactive and non-reactive conformers, has been previously studied using time-resolved stimulated Raman.[12] The reactive conformers showed dynamics forming the ring-closed product extending up to 100 ps. On the other hand, the non-reactive conformers showed transfer of the excited state to a triplet state on a 23 ps time scale.[12]

To gain structural insight into the ring-opening reaction of CHD, we employ femtosecond stimulated Raman spectroscopy (FSRS). FSRS has proven to be a robust method for measuring excited state Raman spectra with high temporal precision (25 fs) and better than 10 cm^{-1} spectral resolution over a broad bandwidth. Previous studies have investigated the reaction mechanisms and excited state vibrational structures of systems such as photoinduced isomerizations,[14,15] excited state proton transfer[15] and charge transfer.[16,17] Moreover, studies of GFP[15] and, more recently, charge transfer dimers[17] have demonstrated the ability to measure two-dimensional or 2D-FSRS spectra which reveal anharmonic coupling in reactive excited states. Our approach is similar to two-dimensional infrared spectroscopy (2D-IR);[18] however, 2D-IR has limited bandwidth, is difficult to extend to excited state systems and, crucially, is blind to the low frequency modes which are of paramount importance for understanding reactivity.[19] Methods such as 6-wave mixing have been developed to measure ground state vibrational anharmonicities.[20]

In this study we impulsively excited ModCHD at 560 nm to launch wave packets in low frequency modes below 250 cm^{-1} and then probed the time dependent excited state structure using fs time resolved stimulated Raman. The time-dependent oscillations in the excited state absorption revealed the low frequency modes along which the excited state wave packet propagates after excitation. This wave packet motion results in remarkable modulations of the intensities and frequencies of the high-frequency excited state FSRS peaks. By analyzing the

oscillations in the excited state FSRS peak center frequencies, we are able to determine quantitative excited state anharmonic couplings between the impulsively excited low frequency modes and the higher frequency Raman active modes. These data provide critical, mode-specific, insight into the vibrational couplings and energy flow that dictate the conrotatory photoreactivity of ModCHD.

Materials and Methods

1,2-bis(2,4-dimethyl-5-phenyl-3-thienyl)perfluoro-cyclopentene (ModCHD, TCI America, >98%) was dissolved in cyclohexane (Fischer, spectroscopic grade) to form solutions of 1 OD per 500 μm at 560 nm (~3 mM) for the FSRS experiments. Prior to the measurements, samples were photoconverted to >90% ring closed ModCHD using a 280-320 nm fluorescent lamp (Philips, UVB Broadband PL-S 9W) and then shielded from exposure to ambient light. Samples were flowed from a 40 mL reservoir using a peristaltic pump through a 500 μm path length cell with a 200 μm quartz window (Starna Cells Inc., 48-Q-0.5-UTWA) at a rate sufficient to replenish the sample volume between laser pulses.

FSRS and ISRS Experiments

The FSRS instrument has been detailed previously.[21] The primary beam is generated by a Ti:sapphire regenerative-amplifier (B.M. Industries, Alpha 1000 US, 991 Hz, 70 fs, 0.91 mJ/pulse, λ_{max} = 790 nm) pumped by a Q-switched Nd:YLF (B.M. Industries, 621-D) and seeded by a home built Kerr lens mode-locked Ti:sapphire oscillator (30 fs 5.3 nJ/pulse, 91 MHz). The output of the regenerative amplifier is split three ways to form the actinic pump, Raman pump, and Raman probe beams. The actinic pump pulse (30 fs, ~200 nJ/pulse, λ_{max} = 560 nm) is generated using a homebuilt non-collinear optical parametric amplifier (NOPA) and compressed using a F2 prism pair (ThorLabs). Filtering 690 mW of the primary beam with a Fabry-Pérot

etalon (TecOptics, Design #A6) produces an optimally shaped ps Raman pump pulse.[22] The resulting beam is further attenuated to yield 100 μJ of 2.8 cm^{-1} bandwidth light centered at 795 nm. The Raman probe pulse is formed by focusing a small portion of the fundamental beam into a 3-mm thick sapphire window to generate a near-IR continuum (7-10 nJ/pulse, 830-940 nm) which is compressed with a BK7 prism pair (CVI Melles Griot). For the ISRS experiments, the beams are generated in the same way as for FSRS but the Raman pump beam is not used.

All three beams are focused into the sample using a 100 mm fl achromatic lens. The Raman pump and Raman probe have parallel polarization and the actinic pump is rotated to the "magic angle" polarization (54.7°) relative to the other two using a half-wave plate (ThorLabs) in order to mitigate rotational effects on the kinetics at longer times. For experiments probing time delays less than 4.5 ps, where these effects are minimal, all beams were polarized parallel for maximum signal to noise. After the sample, the probe beam is spatially filtered from the other two beams using an iris and recollimated using a 100 mm fl lens. The probe beam is dispersed by a spectrograph (Instruments SA, HR320) and each pulse is separately recorded on a CCD camera (Princeton Instruments, PIXIS 100F). For the FSRS experiments, the Raman pump and Raman probe pulses remain temporally locked with the delay chosen for maximum stimulated Raman gain. The delay between the actinic pump and Raman pump/probe is varied by a computer controlled translation stage (Melles Griot, Nanomotion II). For the FSRS experiments, the Raman pump beam is chopped at half the amplifier frequency using a phase locked chopper (Newport, Model 3501) and the stimulated Raman gain is calculated by taking the natural logarithm of Raman-pump-on divided by Raman-pump-off on a shot-to-shot basis. The actinic pump is periodically modulated using an automated shutter (ThorLabs) to take both ground and

excited state Raman spectra. For the ISRS experiment the phase locked chopper is moved to the actinic beam line.

The FSRS difference spectra have had both solvent and ground state signal removed after normalization using the cyclohexane 801 cm^{-1} Raman peak as an internal standard to control for Raman pump power fluctuations. The data were worked up using data analysis software written in IGOR Pro (Wavemetrics).[23]

The FSRS data were taken both with constant 20 fs time steps between -0.5 to 2 ps delay as well in logarithmic steps between -2 and 100 ps. ISRS experiments were taken at 20 fs evenly spaced time delays between -0.5 and 4.5 ps. Spectral energy density analysis of the oscillatory signals in the ISRS and FSRS signals was done with both Fast Fourier Transform (FFT) methods as well as a linear prediction with singular value decomposition (LPSVD) algorithm[24–26] implemented in IGOR Pro.

The instrument response function (IRF) between the actinic pump and Raman probe was measured as the cross correlation in cyclohexane using the Kerr effect (data shown in SI). For FSRS and ISRS the response function had a FWHM of 70 and 77 fs, respectively.

DFT Calculations

Density functional theory (DFT) simulations of the ModCHD molecule were performed using Gaussian 09 to determine the molecular geometry and assign the normal mode character.[27] For both the ground state and first (S_1) excited state, calculations were run using the B3LYP functional and the 6-311++G(D,P) basis set. Ground state nuclear geometries, vibrational frequencies and normal coordinates for both the ring-closed and the ring-open ground state conformers were calculated. The forces exerted on the nuclei by the first and second excited state potentials at the ground state, ring-closed, geometry were calculated using TD-DFT at the

B3LYP/6-311++g(d,p) level. Resonance Raman (RR) intensities were determined from the calculated forces (i.e. slopes) of the excited state potential energy surfaces (PES) along the ground state normal modes.[28]

Results

Figure 2(a) presents the dispersed transient absorption (TA) for ModCHD over the 822-945 nm region from -0.5 to 4 ps after excitation at 560 nm. The induced absorption within the probe window displays three monotonically decaying bands at 830, 875 and 940 nm. Clear oscillations in the contour lines are assigned to impulsively excited vibrations of the ModCHD excited state. Attribution of the signal to excited state, as opposed to impulsively driven ground state, wave packet motion is justified because this spectral region is separated from the ground state bleach by over 200 nm and the signal has a cosine phase consistent with an $S_1 \rightarrow S_n$ transition.[29] Figure 2(b) presents the TA band integral as a function of time (dotted line) along with an exponential fit of the population dynamics (solid line). Figure 2(c) presents the oscillatory component of the signal after removal of the 6020 ± 40 fs population decay (dotted line). The coherence dynamics are fit with an LPSVD algorithm (solid line) between 200 and 2800 fs. Figure 2(d) presents the frequency domain reconstruction of the LPSVD model parameters (solid) as well as the FFT (dotted); there are four intense peaks, at 27, 66, 104, and 191 cm^{-1} with weaker features at 142 and 211 cm^{-1}. Satisfactory agreement between the LPSVD reconstruction and the FFT is observed.

Figure 3 presents the ModCHD excited state stimulated Raman spectra at selected time delays following actinic excitation at 560 nm along with the ground state spectrum. The most intense ground state vibrational resonance is at 1501 cm^{-1} and there are large peaks at 1325, 1439 and 1603 cm^{-1}, which correspond to localized C=C aromatic stretching modes. Additionally,

weaker ground state modes assigned to delocalized C-C aromatic stretches and CH bends are observed at 999, 1036, 1104 and 1158 cm^{-1} along with lower frequency presumably out of plane CH wags at 451 and 593 cm^{-1}. No large dynamic shifts in excited state frequencies are evident in this display of the data but the intensity decreases for all modes from 100 fs to 10 ps; by 30 ps the excited state has fully decayed. Because the ground state depletion signal is very weak compared to the excited state Raman signal at short time delays, it is difficult to observe. However, at 30 ps, after the excited state has decayed, the weak ground state depletion signal can be discerned at the 1325, 1439, and 1501 cm^{-1} ground state frequencies. Time dependence of the ground state depletion signal can be fit with two components, a large 32.5 ps decay component and an extremely slow component that is modeled as a constant offset of 1.6%. The slow component can be assigned to the photochemical ring-opening yield and its magnitude is consistent with previously reported yields of only a few percent for these systems.[10,11]

Figure 4 presents the excited state mode characters with a focus on the central cyclohexadiene ring of ModCHD. Assignments are made in comparison to the ground state DFT calculations using resonant Raman intensities to simulate the excited state resonance conditions. For a large molecule such as ModCHD (59 atoms/282 electrons) the overall spectral shifts caused by exciting a single electron are small enough that simulated ground state vibrational modes can be reliably used to describe the excited state motions. A comparison of the ground and excited state spectra and simulations is presented in Figure S8. Normalized mass weighted displacements are depicted as red arrows. Symmetries are based on the local C_2 point group of the CHD ring. Modes without displacement on the central ring or with symmetry not conforming to C_2 are listed as not applicable. Modes of A-symmetry are of particular note because they project well on to conrotatory excited state motion of the CHD methyl groups depicted at the

bottom. The 27 cm^{-1} mode is primarily a twist of the external phenyl moieties and does not project onto the central ring. The 66 and 104 cm^{-1} modes are symmetric and asymmetric whole molecule bends with A and B symmetry, respectively. The 191 cm^{-1} mode is a totally symmetric CHD methyl wag. The 993 cm^{-1} mode is an aromatic CCC bend of the phenyl groups, the 1580 cm^{-1} mode is a C-C stretch on the peripheral phenyl group with a small displacement on the central ring, and the 1389 cm^{-1} mode is a methyl umbrella mode that does not project well into the C_2 point group. The 467, 1181, and 1333 modes all are localized in the central conjugated framework of ModCHD and have A symmetry. The 467 cm^{-1} mode is a C-C-C bend of the CHD ring and thiophenes, the 1181 cm^{-1} mode is a C-C stretch on the CHD ring and fluorinated pentane and the 1333 cm^{-1} mode is C-C stretch localized on the thiophenes.

Figure 5 presents the intensity decay analysis for the excited state ModCHD Raman modes. The modes are modeled as either a single or double exponential decay between 200 fs and 100 ps. Four characteristic decay rates are observed: ~6 ps (circles), ~3 ps (crosses) and ~0.5 ps (triangles). The TA (open square) fits well to a single exponential decay of 6 ps. The correlation between the timescales of Raman intensity and TA decay suggests that the ~6 ps rate can be assigned primarily to the loss of resonance enhancement as the excited state wave packet moves towards the conical intersection. The ~3 ps timescale has been assigned by previous authors to nuclear wave packet movement over the S_1 transition state[9] and the 0.5 ps decay process is assigned to fast nuclear motion out of the Franck-Condon (FC) region.

More careful examination of the excited state stimulated Raman data with higher time resolution revealed oscillations in both the peak intensities and frequencies. Raman peaks were fit to Lorentzian lineshapes at each time delay and the extracted peak centers and amplitudes were plotted as a function of time. Figure 6 presents four representative vibrational intensity-

frequency trajectories over the first 2 ps for the 467, 1333, and 1580 cm^{-1} modes with 20 fs intervals. The "coherence artifact," which occurs when the actinic pump is coincident with the Raman pump/probe pair, obscures the dynamics for the first 100-200 fs, therefore our analysis focuses on features after 200 fs. Oscillations in both the peak center and amplitude are visible for all four modes although the frequencies of the oscillation are not the same for each peak. On average the peak amplitudes show clear decays for all four modes although there is also a slight rise with a time constant of ~400 fs for the 1580 cm^{-1} mode. For the 1580 cm^{-1} mode the frequency shift mostly occurs during the resonant artifact and there is little change after 300 fs. For the 467 cm^{-1} mode there is a small red shift with an exponential decay constant of ~500 fs, and the 1333 cm^{-1} mode shows blue shift of 4 cm^{-1}.

Figure 7 presents both the time and frequency domain analysis for the peak amplitudes and peak centers of the 1580 cm^{-1} mode. The left side presents the FSRS amplitudes and the peak centers are on the right. The top boxes present the oscillatory signal in the time domain after subtraction of the population decay (dotted) along with an LPSVD fit (solid). The bottom boxes show the frequency domain energy spectral density for both the peak amplitudes and centers using both FFT (dotted) and LPSVD reconstruction (solid). The FFT and LPSVD reconstructions are qualitatively supportive except especially at low frequencies in the frequency analysis. We focus on the results fitting to exponentially damped sinusoids using the LPSVD algorithm because it should result in a significantly more reliable conclusions for cases such as this with increasing noise with long time delay which impacts especially low frequency components.[30] Using a model specific fit of damped sinusoids reduces generalization, but carries large gains in the fidelity of the fit.

For the 1580 cm^{-1} mode, the peak center oscillations have an initial magnitude of 0.8 cm^{-1} and amplitude oscillations of 5 mOD. There is reasonable agreement between the frequencies of the energy spectral density derived from peak amplitudes and those derived from peak centers. Both the peak centers and amplitudes fit to four modes with frequencies of 33, 58, 117, and 193 cm^{-1} and 53, 70, 103, and 210 cm^{-1}, respectively. These data illustrate how the peak amplitude and center frequency of the high frequency modes are modulated by a number of low frequency excited state motions. Hoffman *et al.*[17] have presented evidence that oscillatory features of this type are generated by *intra*molecular 5th order processes as opposed to *inter*molecular 3rd order cascades which have been previously discussed in the literature.[31] Previous studies on molecules with similar photophysics have shown that the amplitude of the SRS frequency oscillatory features are invariant with excited state concentration.[17] Likewise for ModCHD no oscillatory features observed from the cyclohexane solvent, which would be expected if the signal originated from 3rd order cascading Raman signals between the excited state ModCHD and the ground state solvent. Other experiments have shown that the 3rd and 5th order signals can be distinguished by the absolute phase of the signal[20] however because of the signal-to-noise we are refraining from making any conclusions to the fitted phase information in this experiment.

Figure 8 presents a two-dimensional correlation diagram for the 21 observed excited state FSRS peaks and the impulsively excited low frequency modes that modulate them. This analysis is focused on peak center oscillations because they are directly related to molecular structure whereas the peak intensities also depend on electronic resonances. Each circle's ordinate is determined by the FSRS parent peak frequency, the abscissa is the frequency with which that peak's center oscillates and the area of the circle indicates the intrinsic magnitude of the oscillation. For reference, the excited state ISRS data from Figure 3 are shown at the top and the

excited state Raman spectrum at 200 fs delay is shown at the right. The results from the LPSVD were filtered to remove modes with a spectral width less than 3 cm^{-1}. On the one hand the ordinates are, by definition, locked to the frequencies of the 200 fs spectrum (horizontal lines). However it is important to note that the abscissas are determined by the LPSVD fit and are not fixed to the excited state ISRS modes (vertical lines). The intrinsic oscillatory magnitudes presented in Figure 8 are derived from the observed magnitudes by first extrapolating to zero delay and applying two different correction factors. First, a correction is performed to account for the non-negligible temporal width of the instrument response. Second, we correct for the fact that the oscillatory signal is averaged over the vibrational dephasing time.[15,17] The derivations of both correction factors are given in full by Hoffman *et al*.[17] After normalization, the largest intrinsic oscillatory magnitudes are nearly 10% of the high energy peak's vibrational frequency. We also performed an analogous analysis of the oscillatory data using Fourier methods, which is presented in the SI.

These oscillatory signals can be directly related to anharmonic coupling between vibrational degrees of freedom.[17] An estimate of dimensionless anharmonicity between the low and high frequency modes, χ_{LH}, can be made from the equation: $A = -\frac{1}{2}\chi_{LH}\Delta_L$.[17] Here A is the observed relative oscillation magnitude and Δ_L is the dimensionless displacement between the low frequency mode's potential minima in the ground and excited states within the harmonic approximation. Dimensionless displacements can be determined by analysis of resonant Raman intensities (see SI). For instance, the 467 cm^{-1} mode has an intrinsic relative oscillatory magnitude of ~0.1 for the 191 cm^{-1} component and the Δ_{191} was determined to be ~1.0 giving an estimate for $\chi_{191,467}$ of 0.2. This value for χ_{LH} is on the order of magnitude of ground state anharmonic couplings observed in other polyatomic systems.[2]

The largest anharmonic couplings are associated with the 467, 993, 1333, 1389, and 1580 cm^{-1} modes. The most prominent coupling is between the 467 cm^{-1} C-C bending mode and 191 cm^{-1} methyl wag. The 993 cm^{-1} phenyl bend is modulated by 104 cm^{-1} asymmetrical frame bend. The 1333 cm^{-1} C-C stretch oscillates at only 191 cm^{-1} while the 1389 cm^{-1} methyl bend shows oscillations due to the 66, 104 and 191 cm^{-1} modes. The 1580 cm^{-1} phenyl C-C stretching mode is coupled with the 66 and 104 cm^{-1} modes. In general, the modes which couple to the 191 cm^{-1} wag have significant motion in the central cyclohexadiene ring. However, modes which couple to the 66 and 104 cm^{-1} modes are usually more delocalized away from the central CHD system.

To assist discussion, DFT calculations were used to determine which modes most strongly project onto a hypothetical ring opening reaction coordinate (RC). The geometries of the central ring and attached methyl moieties for both the closed and open structures are presented in Figure 9 in a frame of reference without any translation of the center of mass or rotation of the principal axes of inertia. The hypothetical RC is defined to be the linear interpolation between the ring-closed and ring-open geometries, i.e. the RC vector is defined as the difference between the nuclear positions of the closed and open central cyclohexadiene ring only. Figure 9 presents the magnitudes of the projections of the calculated normal coordinates onto the RC as bars below the simulated RR spectrum. The colored dots show which modes are coupled to the 66 cm^{-1} bending (green), 104 cm^{-1} bending (blue) and 191 cm^{-1} methyl wagging (red) modes (see Figure 8). Most modes between 200 and 600 cm^{-1} are parallel to the predicted RC. Between 800 and 1303 cm^{-1} only a few modes are significantly aligned with the RC and most modes greater than 1309 cm^{-1} are primarily orthogonal to the RC even though the RR intensities (see SI) demonstrate that they are highly displaced in the excited state. The 1389 cm^{-1} Me-bend and 1580 cm^{-1} phenyl C=C modes, which couple to the 66 cm^{-1} mode (green), also do not show significant motion along the

RC. Of all the modes that are coupled to the 104 cm^{-1} mode (blue)–993, 1389, and 1580 cm^{-1}–only the 993 cm^{-1} mode is aligned with the predicted RC. Interestingly, all modes coupled to the 191 cm^{-1} methyl wag motion (red)–467, 1181, and 1333 cm^{-1}–show significant motion parallel to the RC.

Discussion

Time resolved excited state stimulated Raman spectra have provided new information on the structural dynamics that occur during the ring opening reaction of a modified cyclohexadiene including the quantitative measurement of the excited state vibrational anharmonic couplings that report on the shape of reactive potential energy surfaces. Impulsive photoexcitation of ModCHD at 560 nm launches a wave packet on the excited state surface that leads to oscillatory modulation of the excited state absorption because of the highly displaced 27, 66, 104, and 191 cm^{-1} low frequency modes. Conventional time resolved excited state FSRS spectra of excited ModCHD reveal twenty-one intense excited state Raman modes that decay with three characteristic timescales: fast nuclear motion out of the FC region (~0.5 ps), passage through the transition state (TS) (~3 ps) and subsequent loss of electronic resonance as the system evolves towards the conical intersection (~6 ps). However, more careful examination of the high frequency excited state stimulated Raman peak frequencies and amplitudes reveals that they oscillate at the 66, 104 and 191 cm^{-1} torsion and methyl twist frequencies demonstrating large anharmonic coupling between a number of the high and low frequency modes in ModCHD. Quantitative analysis of the frequency oscillations reveals the magnitude of the mode-specific anharmonic coupling. In particular, the strong anharmonic coupling between the methyl wagging mode and the CC stretch and CCC bend in the CHD ring moiety is critical for understanding how the ModCHD conrotatory ring-opening reaction proceeds.

To interpret our results, we explore the correlations between different mode properties such as character, rate of intensity decay and projection onto the hypothetical RC. Both the 467 cm^{-1} CCC bend and 1333 cm^{-1} C-C stretch modes have a quick (~3 ps) intensity decay, reactive A symmetry and are localized to the central reactive cyclohexadiene ring. Moreover, both modes show the strongest anharmonic coupling to the 191 cm^{-1} conrotatory, CHD localized, methyl wag. On the other hand, the 993 cm^{-1} phenyl bend and the 1580 cm^{-1} phenyl stretches all decay more slowly (~6 ps), have characters that are either localized away from the central ring or have poor projection into the C_2 point group and consist of motion orthogonal to the predicted RC. The 993 cm^{-1} mode shows anharmonic coupling to the 104 cm^{-1} mode, and the 1580 cm^{-1} mode shows coupling to both the 66 and 104 cm^{-1} frame bends which are delocalized away from the reactive ring. Based on this correlation of characteristics, we can partition the modes into two groups that we term "reactive" and "unreactive." Of the modes that show strong couplings, the 191, 467, and 1333 cm^{-1} modes exhibit reactive behavior while the 66, 104, 993, and 1580 modes can all be categorized as non-reactive. For completeness, two modes have characteristics in common with both groups: the 1181 and 1389 cm^{-1} modes are coupled to all three of the 66, 104, and 191 cm^{-1} modes though some of these couplings are weak.

The reactive and unreactive labels can be understood in the context of the predictions made by Woodward and Hoffman for pericyclic rearrangement.[5] For 1,3-cyclohexadiene, the mechanism of photoactivated ring-opening is a conrotatory A-type motion of the alkane hydrogens (see Figure 4).[6,32] Therefore we assign the group with A-symmetry as "reactive" because they contribute to an overall conrotatory motion consistent with the mechanism of photoinduced ring breaking. The remaining modes do not have a reactive A symmetry and have significant motion on the external phenyl moieties suggesting that they funnel energy out of the

initially excited high frequency FC active modes and away from the reactive center thereby playing a crucial role in non-reactive internal conversion. Parasitic non-reactive pathways have been previously identified by *ab intio* calculations to be accessible before the molecule crosses the excited state TS.[9]

To understand how the molecule approaches and crosses the TS we focus on the product-forming reactive modes. Reactive coordinates involved in crossing the TS are, by definition, anharmonic at and near the TS; it is therefore expected that the reactive modes will be strongly anharmonically coupled to one another as they distort towards the TS. The 191 cm^{-1} motion symmetrically distorts the CHD methyls but does not significantly perturb the bond order of the ring. The 467 cm^{-1} CCC bend reduces the bond order between the ring opening carbons. The 1333 cm^{-1} C-C stretch mode (also strongly coupled to the 191 cm^{-1} mode) distorts the top C-C single bond on the CHD ring. All three of these modes show similar motions on the central ring and project strongly onto the predicted reaction coordinate. These properties are self-consistent and strongly suggest that these modes make a significant contribution to the motion necessary to cross the product forming TS.

Our results are in general agreement with previous reports on ModCHD and similar photoswitches. Kinetic decay rates of ModCHD observed here are consistent with those observed previously by transient absorption.[10] Besides the reactive pathways that funnel the excited state through the conical intersection, previous authors[9,11] have identified alternative non-reactive pathways. Here, we have demonstrated that these non-reactive pathways are dominated by motion on the peripheral phenyl moieties. Anharmonic couplings allow energy to be transferred from the initially excited degrees of freedom, such as the high frequency ethylenic modes to lower frequency modes that may be reactive or simply peripheral energy loss pathways.

The relative magnitude between the anharmonic couplings to modes that promote reaction and to those that do not determines the overall yield of the reaction. The coupling pattern observed in Figure 8 indicates that for ModCHD the ethylenic excitation is very efficiently degraded into non-reactive vibrational pathways.

Previous work on CHD has identified ballistic motion along the symmetric C=C twist, CH_2-CH_2 stretch, and a CH_2 twist after photoexcitation driving conrotatory cycloreversion[6,33]. Our work shows that ModCHD undergoes a similar coherent nuclear motion that is responsible for the reaction even though ModCHD reacts much slower. Femtosecond Raman spectroscopy therefore allows us to identify the specific molecular motions that define the initial stages of molecular reactivity. 2D-FSRS also allows us to determine the vibrational anharmonicities that help to parse the initial Franck-Condon excitation between reactive and nonreactive pathways and that determine energy relaxation rates.

In conclusion, 2D-FSRS of ModCHD has revealed reactively important couplings between normal modes that are in excess of 40 cm^{-1}. Based on the correlations of these couplings with other key properties, we deduce that the 191 cm^{-1} methyl wag mode is a critical molecular deformation in the initial stages of the ring opening reaction, and that the transition state involves a highly mixed combination of the 191 methyl wag, the 467 cm^{-1} C-C bend and the 1333 cm^{-1} C-C stretch. On the other hand, the 66 and 104 cm^{-1} modes appear to be non-reactive motions that compete effectively with the reactive ones for energy leading to the low quantum yield of this molecule. With shorter actinic pulses and an optimally chosen Raman pump, it should ultimately be possible to use 2D-FSRS to reveal anharmonic couplings between all Raman active degrees of freedom, independent of frequency. The resulting quantitative measurement of excited state inter-mode anharmonic couplings will be crucial for improving our understanding of all types of

photoreactive phenomena including isomerization, atom transfer, energy transfer, electron transfer and internal conversion.

Acknowledgements

Financial support was provided by the Mathies Royalty Fund. We would like to thank Kathy Durkin of the Molecular Graphics and Computation Facility for assistance with the simulation results (NSF CHE-0840505).

References

(1) Bernardi, F.; Olivucci, M.; Robb, M. A. *Chem. Soc. Rev.* **1996**, *25*, 321.
(2) Hamm, P.; Lim, M.; Hochstrasser, R. M. *J. Phys. Chem. B* **1998**, *102*, 6123.
(3) Dunkelberger, E. B.; Woys, A. M.; Zanni, M. T. *J. Phys. Chem. B* **2013**, *117*, 15297.
(4) Deb, S.; Weber, P. M. *Annu. Rev. Phys. Chem.* **2011**, *62*, 19.
(5) Woodward, R. B.; Hoffmann, R. *Angew. Chem. Int. Ed. Engl.* **1969**, *8*, 781.
(6) Reid, P. J.; Lawless, M. K.; Wickham, S. D.; Mathies, R. A. *J. Phys. Chem.* **1994**, *98*, 5597.
(7) Irie, M. *Chem. Rev.* **2000**, *100*, 1683.
(8) Browne, W. R.; Feringa, B. L. *Annu. Rev. Phys. Chem.* **2009**, *60*, 407.
(9) Boggio-Pasqua, M.; Ravaglia, M.; Bearpark, M. J.; Garavelli, M.; Robb, M. A. *J. Phys. Chem. A* **2003**, *107*, 11139.
(10) Ward, C. L.; Elles, C. G. *J. Phys. Chem. Lett.* **2012**, *3*, 2995.
(11) Ishibashi, Y.; Umesato, T.; Kobatake, S.; Irie, M.; Miyasaka, H. *J. Phys. Chem. C* **2012**, *116*, 4862.
(12) Pontecorvo, E.; Ferrante, C.; Elles, C. G.; Scopigno, T. *J. Phys. Chem. B* **2014**, *118*, 6915.
(13) Weigel, A.; Ernsting, N. P. *J. Phys. Chem. B* **2010**, *114*, 7879.
(14) Hoffman, D. P.; Mathies, R. A. *Phys. Chem. Chem. Phys.* **2012**, *14*, 6298.
(15) Fang, C.; Frontiera, R. R.; Tran, R.; Mathies, R. A. *Nature* **2009**, *462*, 200.
(16) Fujisawa, T.; Creelman, M.; Mathies, R. A. *J. Phys. Chem. B* **2012**, *116*, 10453.
(17) Hoffman, D. P.; Ellis, S. R.; Mathies, R. A. *J. Phys. Chem. A* **2014**, *118*, 4955.
(18) Khalil, M.; Demirdöven, N.; Tokmakoff, A. *J. Phys. Chem. A* **2003**, *107*, 5258.
(19) Fayer, M. D. *Annu. Rev. Phys. Chem.* **2009**, *60*, 21.
(20) Molesky, B. P.; Giokas, P. G.; Guo, Z.; Moran, A. M. *J. Chem. Phys.* **2014**, *141*, 114202.
(21) McCamant, D. W.; Kukura, P.; Yoon, S.; Mathies, R. A. *Rev. Sci. Instrum.* **2004**, *75*, 4971.
(22) Hoffman, D. P.; Valley, D.; Ellis, S. R.; Creelman, M.; Mathies, R. A. *Opt. Express* **2013**, *21*, 21685.
(23) Hoffman, D. P. Igor-Data-Analysis https://github.com/david-hoffman/Igor-Data-Analysis (accessed Jul 15, 2013).
(24) Tufts, D.; Kumaresan, R. *IEEE Trans. Acoust. Speech Signal Process.* **1982**, *30*, 671.
(25) Barkhuijsen, H.; de Beer, R.; Bovée, W. M. M. J.; van Ormondt, D. *J. Magn. Reson. 1969* **1985**, *61*, 465.
(26) Barkhuijsen, H.; de Beer, R.; van Ormondt, D. *J. Magn. Reson. 1969* **1986**, *67*, 371.
(27) Frisch, M. J.; Trucks, G. W.; Schlegel, H. B.; Scuseria, G. E.; Robb, M. A.; Cheeseman, J. R.; Scalmani, G.; Barone, V.; Mennucci, B.; Petersson, G. A.; Nakatsuji, H.; Caricato, M.; Li, X.; Hratchian, H. P.; Izmaylov, A. F.; Bloino, J.; Zheng, G.; Sonnenberg, J. L.; Hada, M.; Ehara, M.; Toyota, K.; Fukuda, R.; Hasegawa, J.; Ishida, M.; Nakajima, T.; Honda, Y.; Kitao, O.; Nakai, H.; Vreven, T.; Montgomery, Jr., J. A.; Peralta, J. E.; Ogliaro, F.; Bearpark, M.; Heyd, J. J.; Brothers, E.; Kudin, K. N.; Staroverov, V. N.; Kobayashi, R.; Normand, J.; Raghavachari, K.; Rendell, A.; Burant, J. C.; Iyengar, S. S.; Tomasi, J.; Cossi, M.; Rega, N.; Millam, N. J.; Klene, M.; Knox, J. E.; Cross, J. B.; Bakken, V.; Adamo, C.; Jaramillo, J.; Gomperts, R.; Stratmann, R. E.; Yazyev, O.; Austin, A. J.; Cammi, R.; Pomelli, C.; Ochterski, J. W.; Martin, R. L.; Morokuma, K.; Zakrzewski, V. G.; Voth, G. A.; Salvador, P.; Dannenberg, J. J.; Dapprich, S.; Daniels, A. D.; Farkas, O.;

Foresman, J. B.; Ortiz, J. V.; Cioslowski, J.; Fox, D. J. *Gaussian 09, Revision A.1*; Gaussian, Inc.: Wallingford, CT, 2009.
(28) Guthmuller, J.; Champagne, B. *J. Chem. Phys.* **2007**, *127*, 164507.
(29) Pollard, W. T.; Lee, S.-Y.; Mathies, R. A. *J. Chem. Phys.* **1990**, *92*, 4012.
(30) Eom, I.; Yoon, E.; Baik, S.-H.; Lim, Y.-S.; Joo, T. *Opt. Express* **2014**, *22*, 30512.
(31) Mehlenbacher, R. D.; Lyons, B.; Wilson, K. C.; Du, Y.; McCamant, D. W. *J. Chem. Phys.* **2009**, *131*, 244512.
(32) De Kock, R. J.; Minnaard, N. G.; Havinga, E. *Recl. Trav. Chim. Pays-Bas* **1960**, *79*, 922.
(33) Kosma, K.; Trushin, S. A.; Fuß, W.; Schmid, W. E. *Phys. Chem. Chem. Phys.* **2008**, *11*, 172.

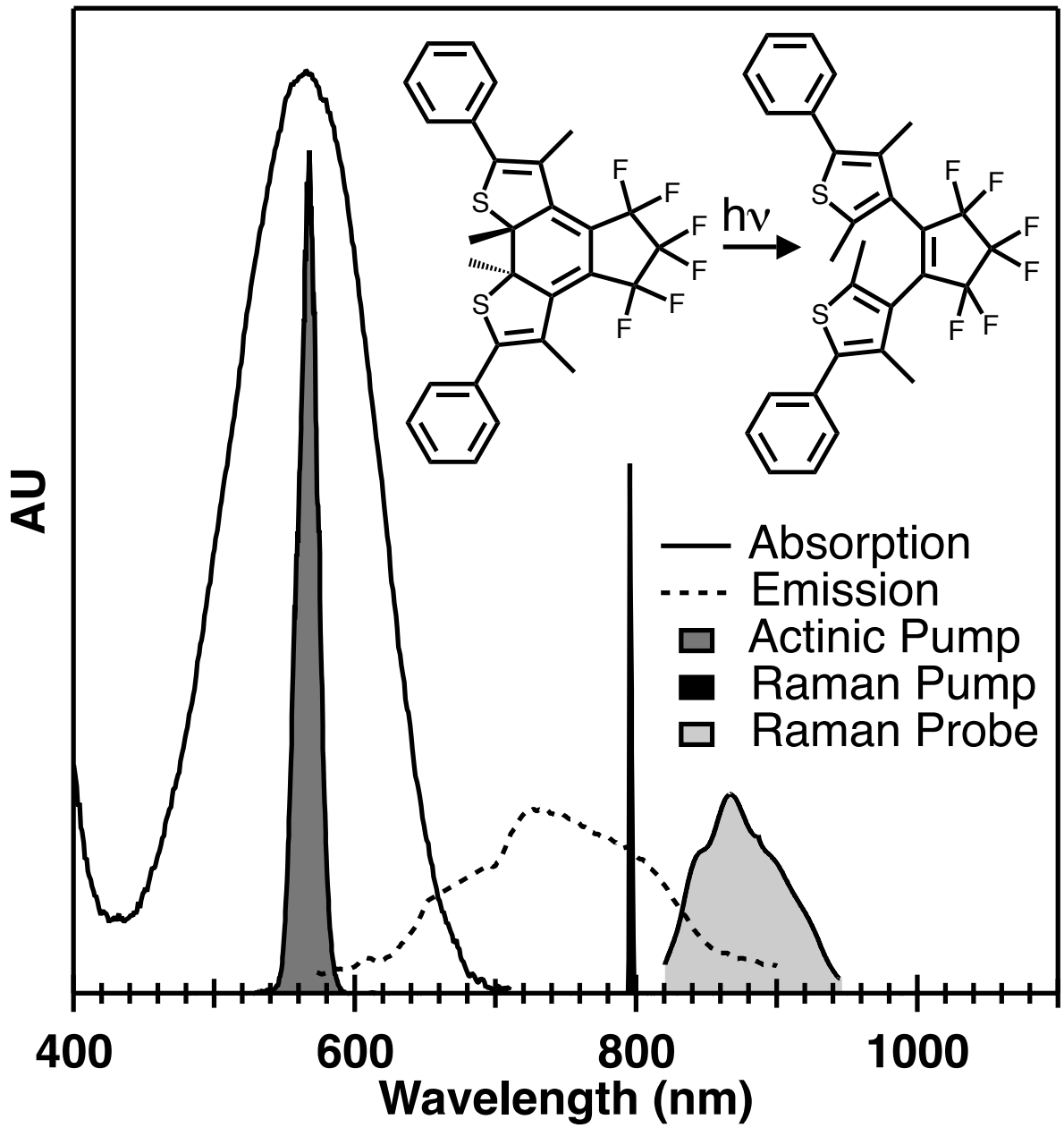

Figure 1. Structure of 1,2-bis(2,4-dimethyl-5-phenyl-3-thienyl)-3,3,4,4,5,5-hexafluoro-1-cyclopentene (ModCHD) and absorption (solid) and emission (dotted) spectra along with the spectra of the three beams used in the FSRS experiment: the actinic pump centered at 560 nm (dark gray), the Raman pump centered at 795 nm (black) and the Raman probe (830-940 nm, light gray). The photochemical ring opening is also depicted.

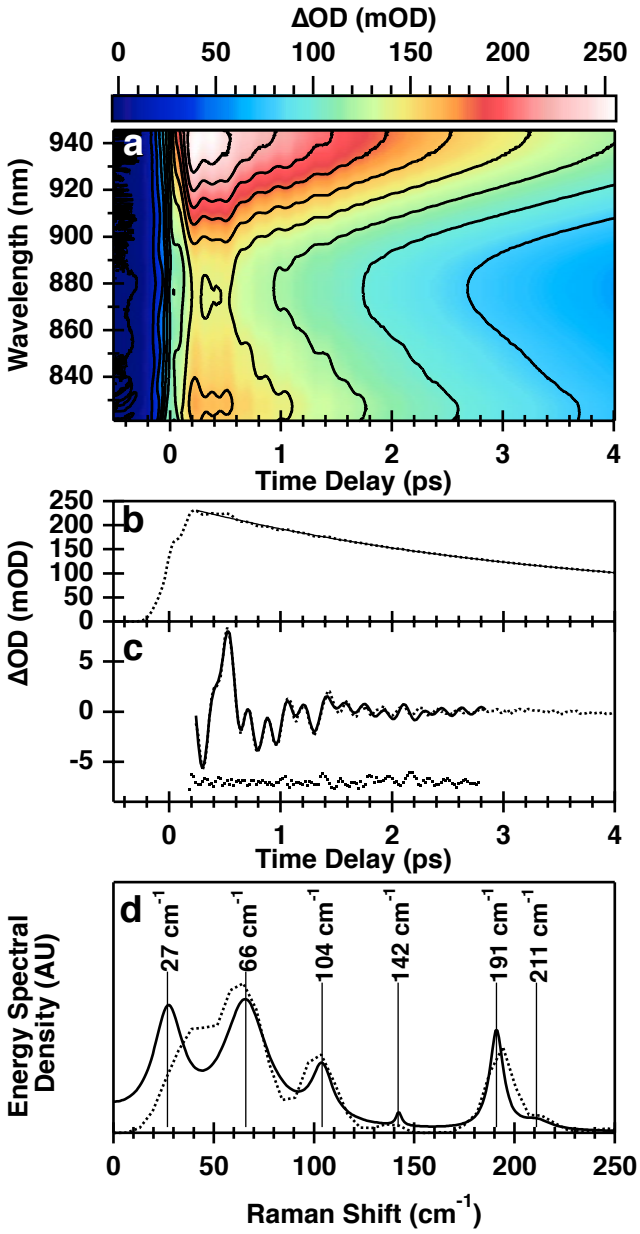

Figure 2. (a) Dispersed transient absorption (TA) in the 822-945 nm region from -0.5 to 4 ps. (b) TA integrated over the full window (dotted) and multi-exponential fit (solid). (c) Oscillatory component after removal of the population decay (dotted), LPSVD fit (solid), and fit residual (dotted, below). (d) LPSVD (solid) and FFT (dotted) energy spectral densities of the oscillatory component. LPSVD central frequencies are indicated.

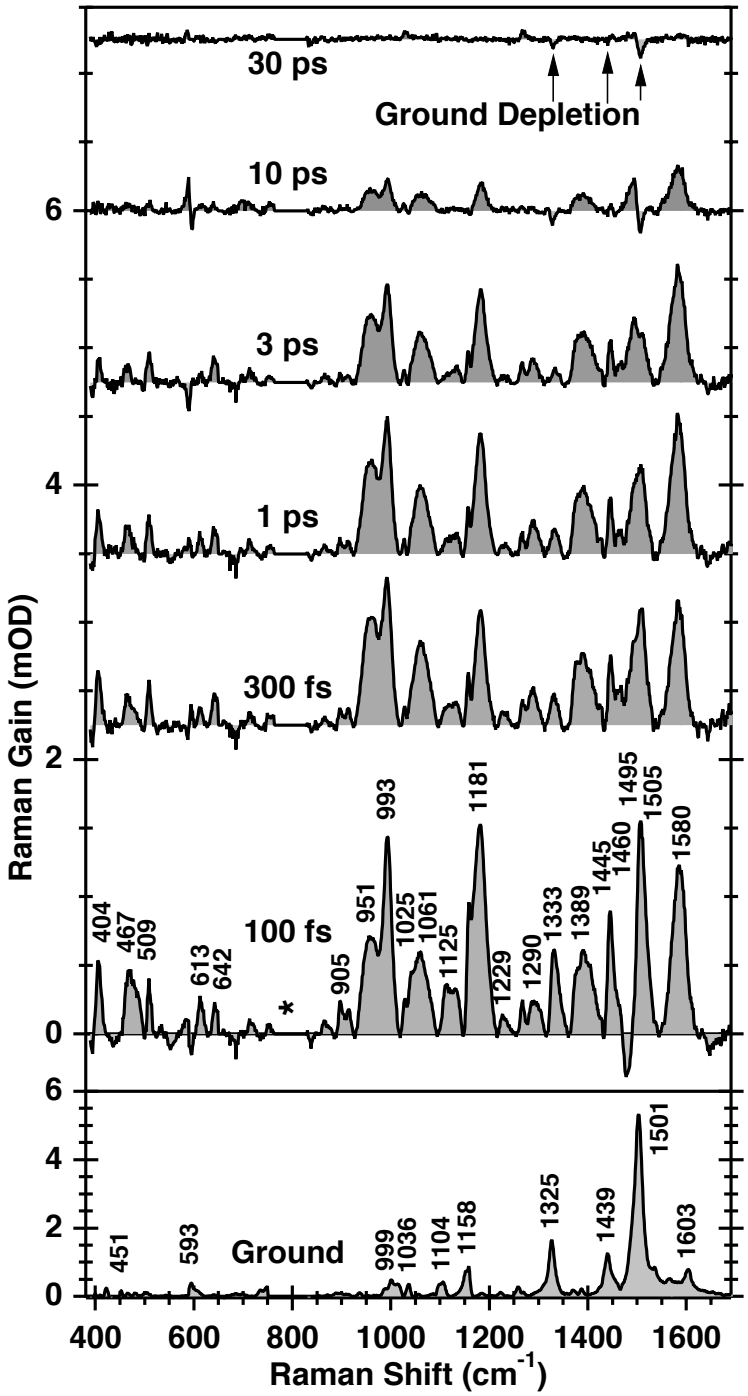

Figure 3. Selected excited state stimulated Raman spectra of ModCHD at the indicated time delays with 795 nm Raman pump and 822-945 nm Stokes probe. Mode frequencies are shown at top. The negative feature at ~1500 cm^{-1} in the 30 ps trace is assigned to ground state depletion. The stimulated Raman spectrum of the ground state is shown at the bottom for comparison.

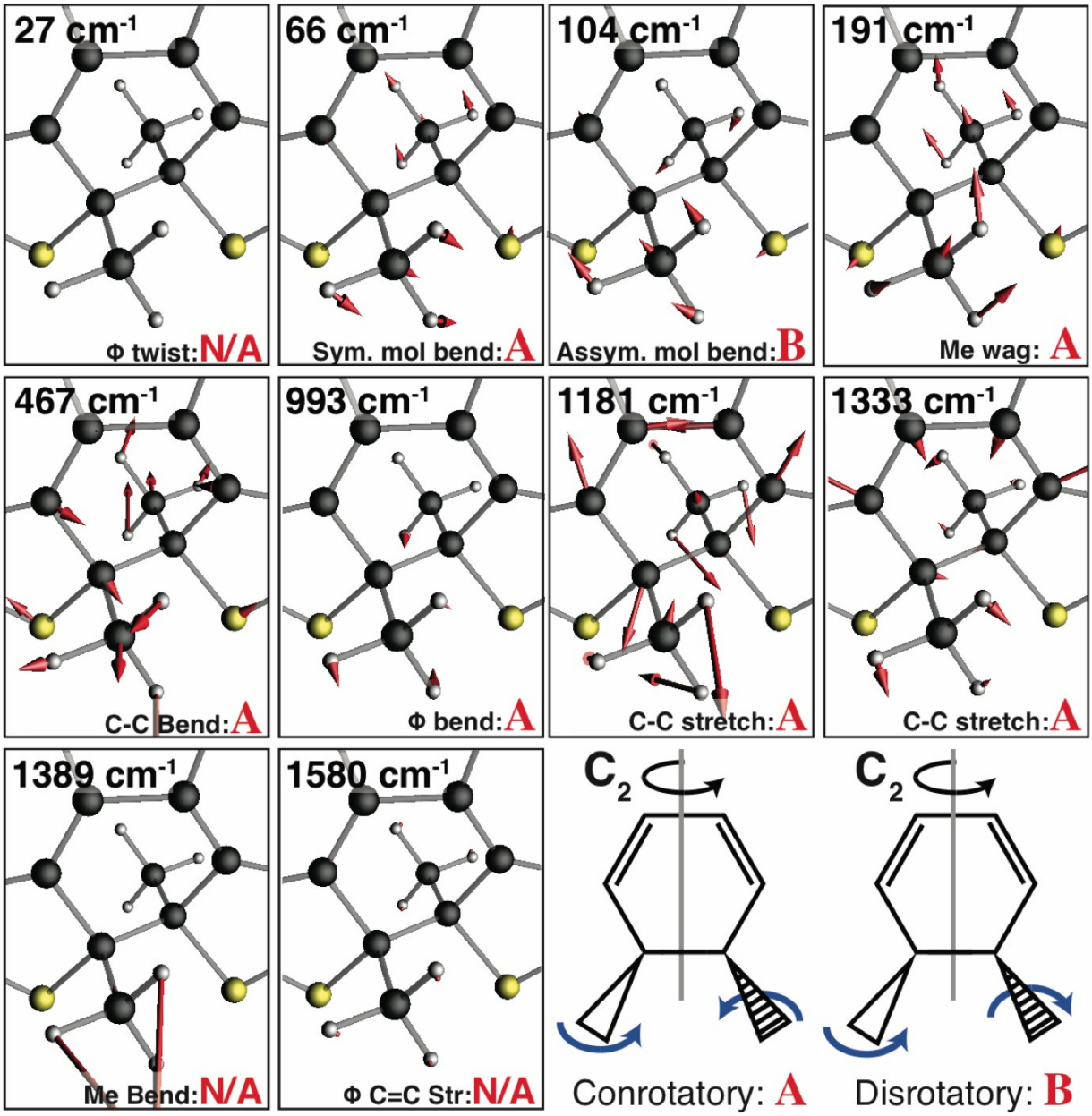

475 **Figure 4:** Assignments for prominent excited state FSRS modes of ModCHD. Red vectors
476 indicate the mass weighted displacement of the normal modes on the central cyclohexadiene ring.
477 For each mode the point symmetry of the vibrations on the central ring projected onto the C_2
478 basis is indicated. Modes are labeled either A or B symmetry or not applicable (N/A) for the
479 modes that either do not project into C_2 or are not localized on the central ring. The sketches in
480 the bottom right show the A symmetry conrotatory and B symmetry disrotatory opening of the
481 central ring. Ground state normal mode displacements whose frequencies best correspond to the
482 indicated excited state frequencies are presented.
483

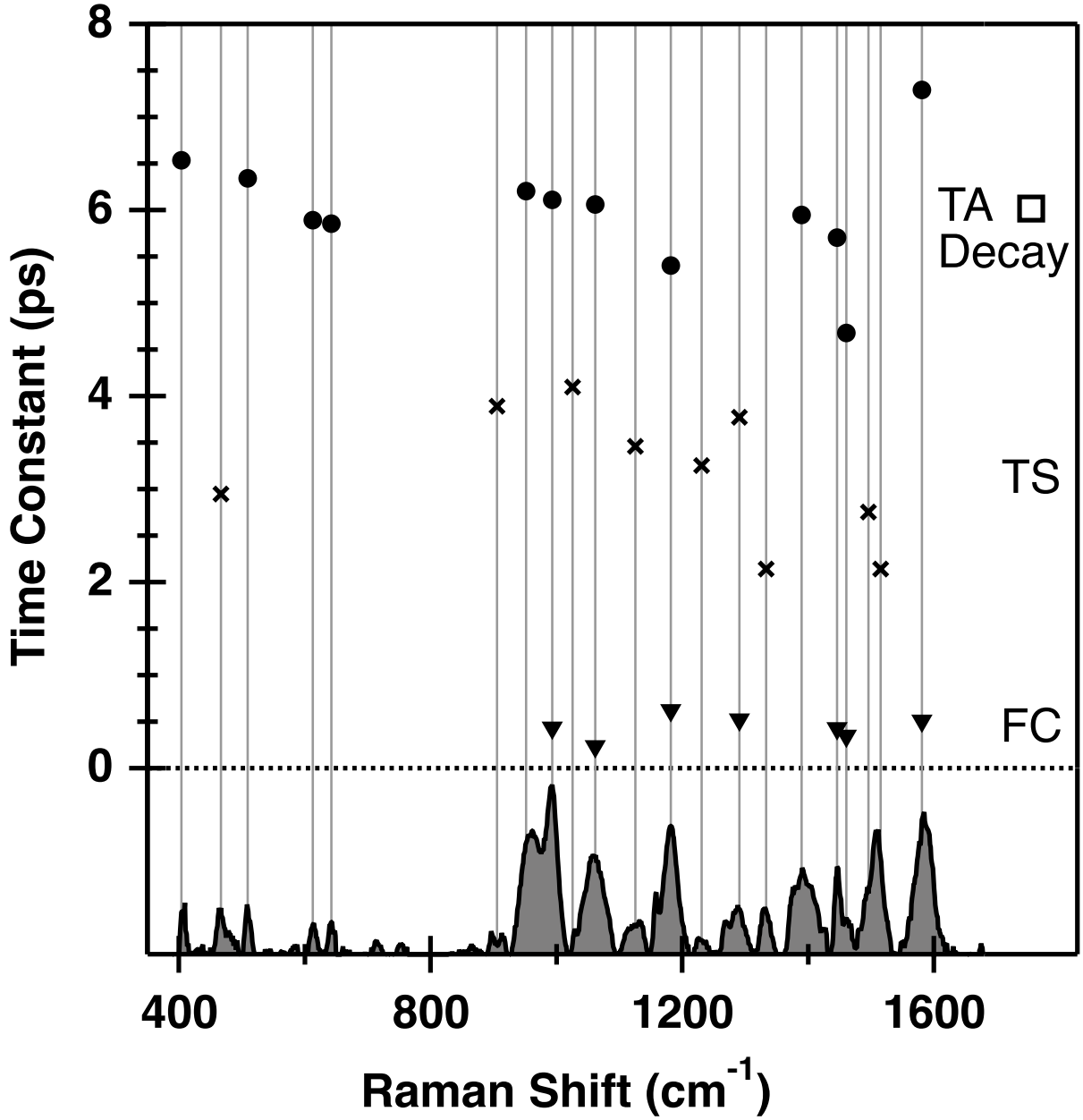

Figure 5. Exponential decay constants of the ModCHD excited state modes as well as the transient absorption. The FSRS excited state modes are fit to single or double exponential decays with the different symbols indicating decays of ~6 ps (circles), ~3 ps (crosses) and ~0.5 ps (triangles). The open square shows the decay rate for the transient absorption. The excited state Raman spectrum at 200 fs delay is shown below for comparison.

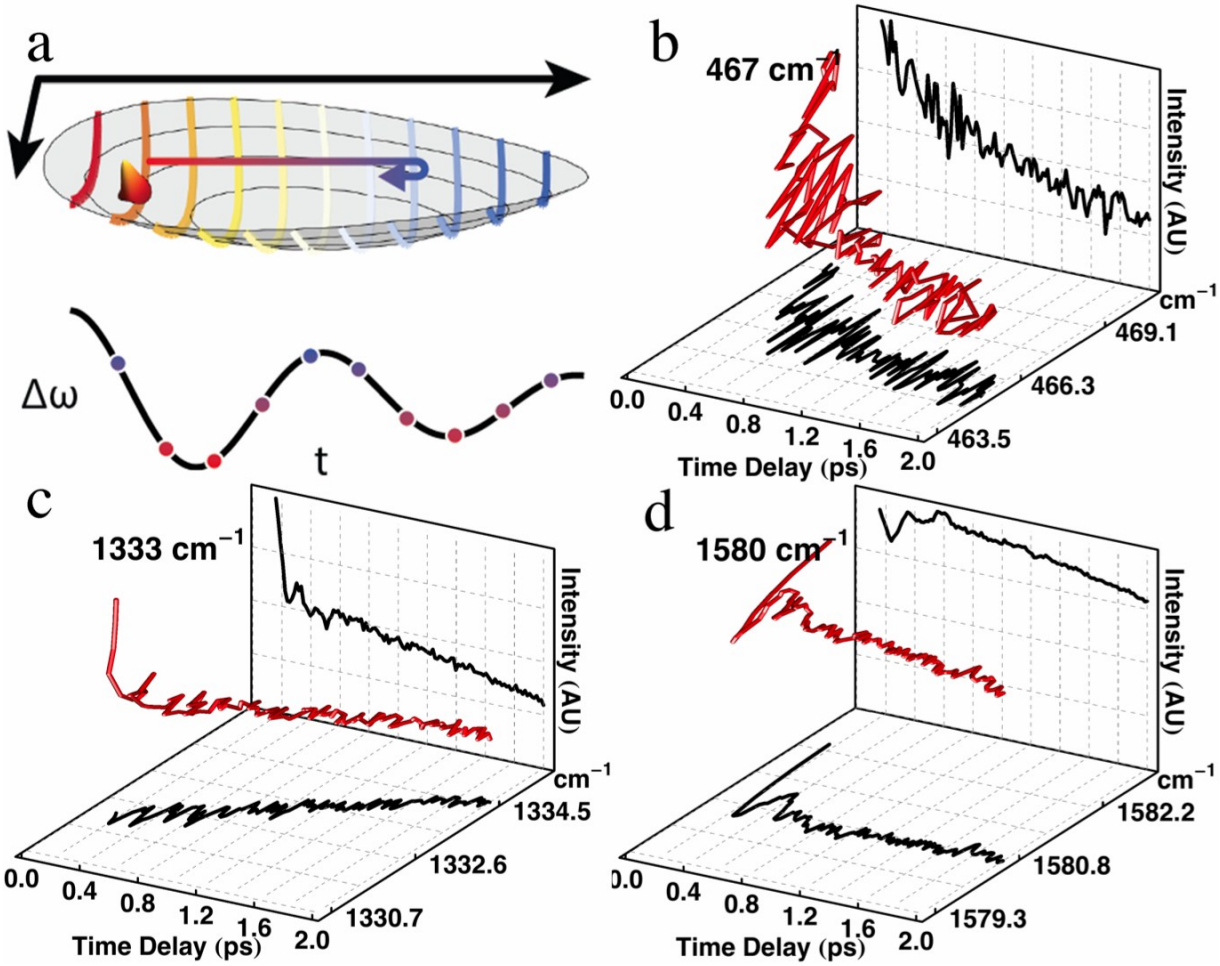

Figure 6. a: Schematic two dimensional potential energy surface where the force constant of the high frequency oscillator depends on the displacement of the low frequency mode. The corresponding plot depicts the modulation of the high frequency mode frequency by wavepacket motion along the low frequecy mode. b-d: Intensity-frequency trajectories for the 467, 1333, and 1580 cm^{-1} excited state peaks of ModCHD. Each plot shows the peak's Raman shift and intensity at 20 fs intervals. Peak parameters were extracted using a Lorenztian lineshape model. Projections of the intensity and Raman shift are shown behind and below, respectively.

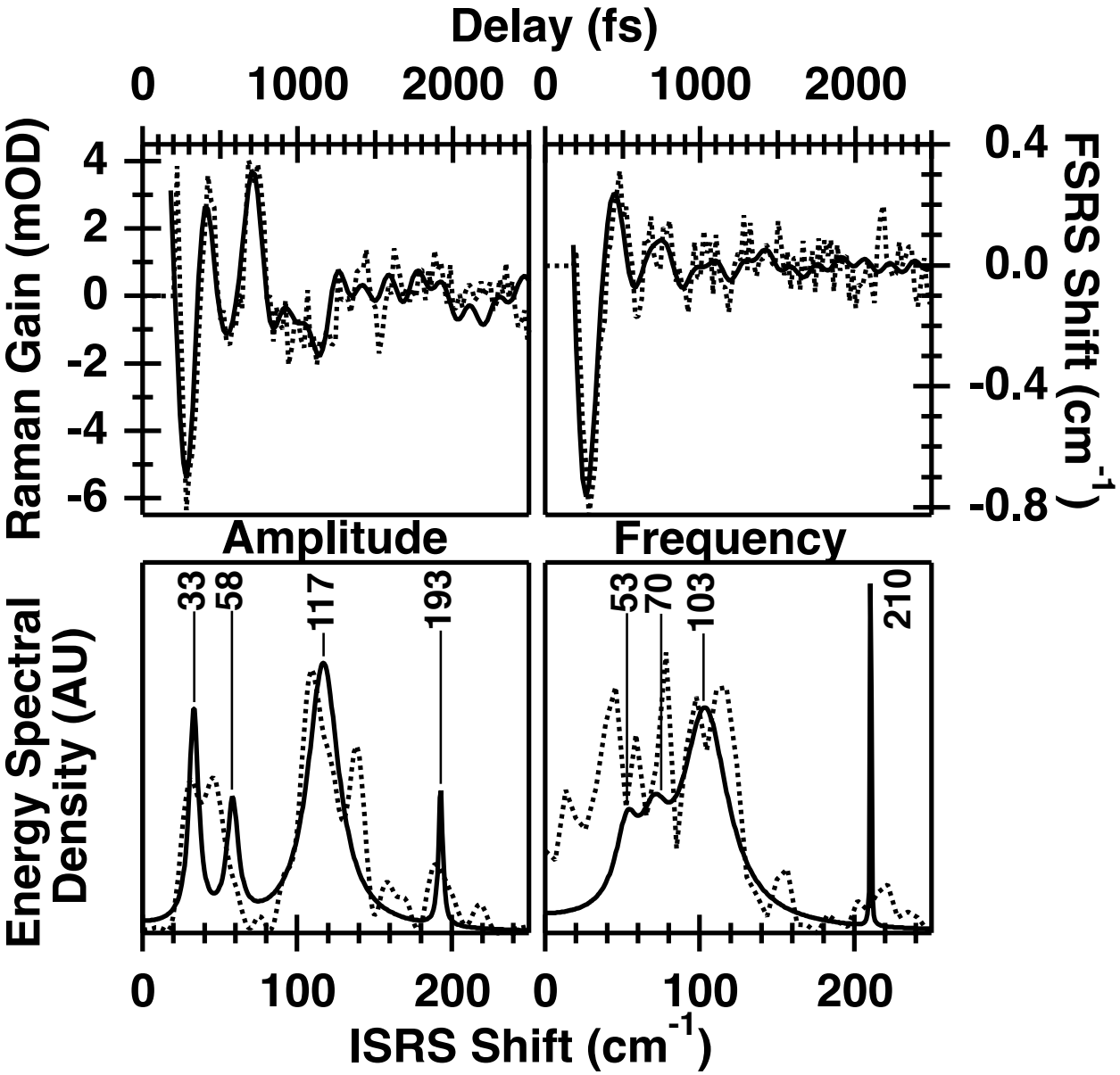

Figure 7. Top Panels: The oscillatory 1580 cm^{-1} peak intensities (left) and Raman shifts (right) taken from 200 to 2,500 fs after removal of the population dynamics (dotted lines) and LPSVD fits (solid lines). Bottom Panels: FFT of the residuals (dotted) and LPSVD reconstructions (solid).

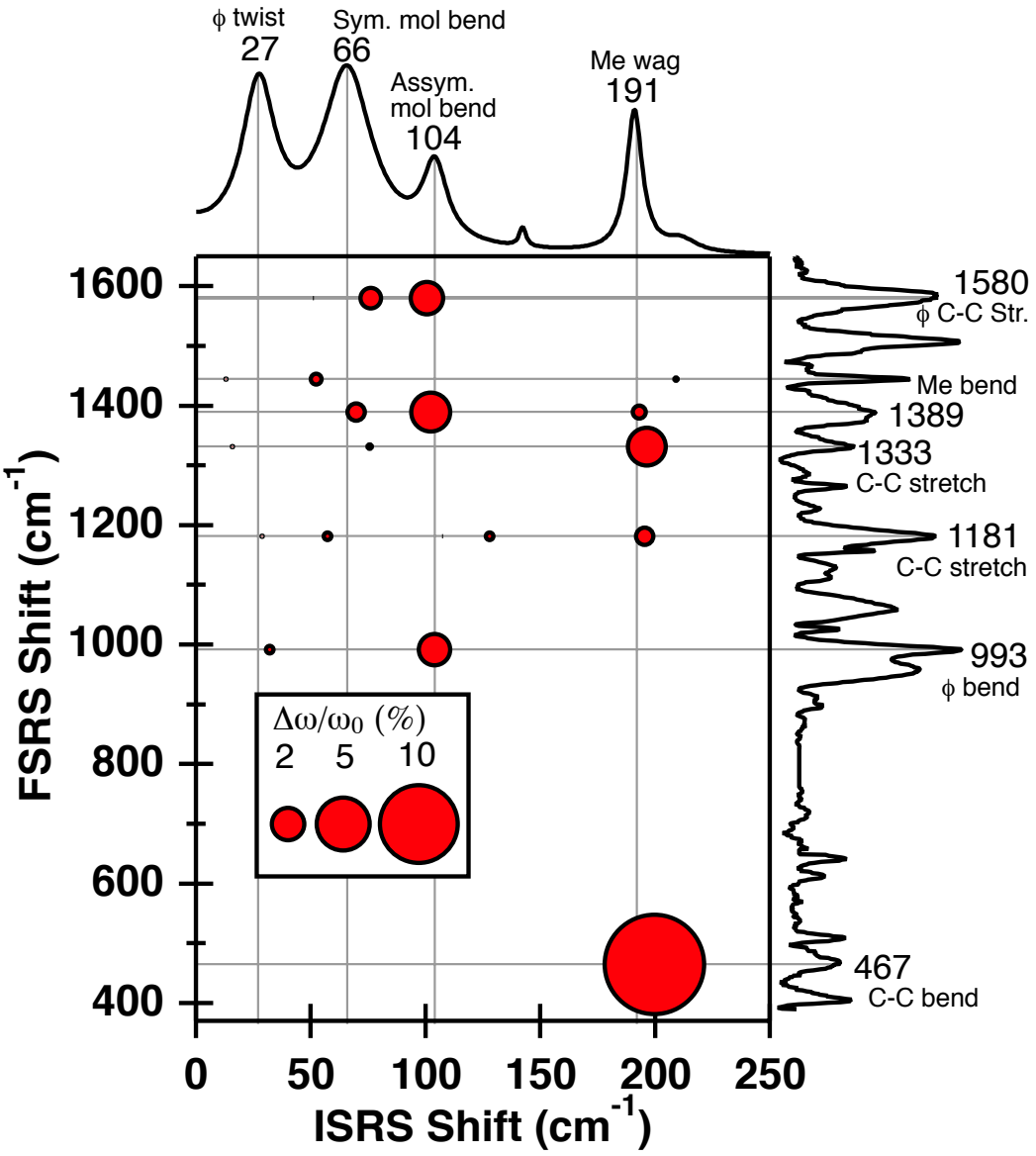

Figure 8. Anharmonicity correlation diagram between excited state FSRS modes and low frequency impulsive stimulated Raman modes. A stimulated Raman spectrum of the excited state of ModCHD at 200 fs delay is shown at right. The excited state ISRS spectrum from Figure 2(d) is shown at top. The circles' ordinates and abscissas indicate FSRS average frequency and FSRS peak center oscillation, respectively. The areas of the circles represent the intrinsic relative magnitudes of the oscillations that range from 2 to 10%.

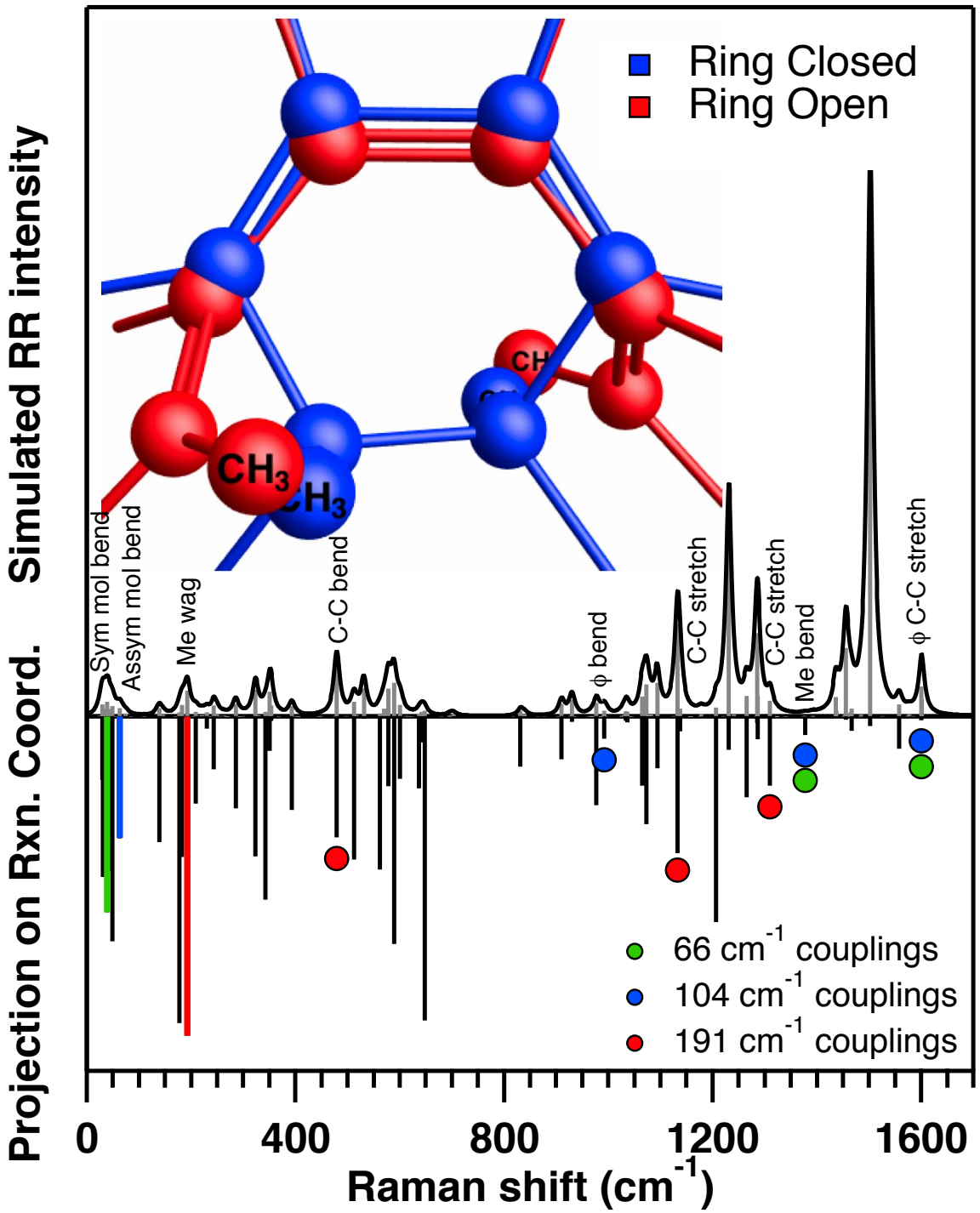

Figure 9: Top: The optimized geometries for ring-closed (blue) and ring-open (red) ModCHD central rings. Middle: DFT simulated resonance Raman spectrum. Bottom: Projection of ModCHD normal modes onto the hypothetical reaction coordinate with arbitrary scaling. Green, blue and red dots indicate modes coupled to the 66, 104, and 191 cm^{-1} modes, respectively. The Raman shift frequencies correspond to the DFT calculated frequencies.